Journal of Applied Fluid Mechanics, Vol. 17, No. 12, pp. 2623-2636, 2024.
Available online at www.jafmonline.net, ISSN 1735-3572, EISSN 1735-3645.
https://doi.org/10.47176/jafm.17.12.2742

Effect of Permeability and Length of a Perforated Splitter Plate Downstream of the Circular Cylinder

S. Sahin[1], T. Durhasan[2], E. Pınar[1] and H. Akıllı[1†]

[1] *Çukurova University, Mechanical Engineering Department, Adana, Turkey*
[2] *Adana Alparslan Türkeş Science and Technology University Aerospace Engineering, Adana, Turkey*

†Corresponding Author Email: hakilli@cu.edu.tr

ABSTRACT

Extensive research has been conducted on the flow control of bluff bodies to address negative impacts such as vibration, acoustic noise, and resonance caused by wake flow. The circular cylinder, due to its simple geometry, is frequently studied as a bluff body and is utilized in various engineering applications including cooling system pipes, electrical pylons, industrial flue systems, overpasses, satellite antennas, electrical cables, and marine drilling platforms. In this investigation, a perforated splitter plate was strategically positioned at different downstream locations to manage the wake flow of the cylinder. The experiments were conducted in a sophisticated, closed-loop water channel at the Fluid Mechanics Laboratory of Cukurova University, providing a controlled environment for precise flow analysis. To measure the instantaneous velocity vector field in the wake region of the cylinder at a Reynolds number (Re) of 5000 (based on the cylinder diameter, D), particle image velocimetry (PIV) was employed. Three different permeability values for the splitter plate (e=0.30, 0.50, 0.70) and three lengths (ls*=1, ls*=2, ls*=3) were tested, maintaining a constant gap (G/D=1) between the splitter plate's leading edge and the cylinder surface. The splitter plates were aligned with the flow direction (Θ=0°). The permeable separator plates minimize the interaction of boundary layers formed around the cylinder, enhancing their effect in downstream regions where shear layer interaction is more pronounced. Consequently, this results in reduced fluctuations and a more stabilized wake flow downstream of the cylinder.

Article History

Received March 25, 2024
Revised June 24, 2024
Accepted July 16, 2024
Available online October 2, 2024

Keywords:

Cylinder
Flow Control
Perforated Splitter Plate
PIV

1. INTRODUCTION

Flow around submerged objects is a common occurrence in a variety of engineering applications, such as cooling system ducts, utility poles, industrial smokestacks, highway overpasses, satellite communication antennas, electrical transmission lines, offshore drilling platforms, and more. The significance of this flow becomes apparent when periodic vortex shedding occurs behind the bluff body. This shedding creates periodic forces that lead to structural vibrations, acoustic noise, and resonance. These adverse effects are undesirable from an engineering perspective and should be minimized.

To control the flow behind the bluff body, both active and passive flow control methods are employed. Active methods involve introducing external energy into the flow field, such as flow suction and blowing (Chen, 2013), feedback control (Fujisawa, 2001), electromagnetic control (Weier, 1998), oscillation of cylinders (Guilmineau, 2002), heating (Lecordier et al., 1991), acoustic excitations (Blevins, 1985), and plasma actuators (Tabatabaeian, 2015). Passive methods alter the bluff body's shape or incorporate additional geometries, such as surface protrusions (Favier et al. 2009), control cylinders (Özdil, 2013), and splitter plates (Roshko, 1954).

A splitter plate {XE "splitter plate:"} is a passive control device which can be installed in the upstream, downstream or both with different arrangements and numbers. Splitter plates might be attached or detached to the body surface. The main idea is to isolate the flow separation behind the structure. Firstly, Roshko (1954) made a series of experiments to illustrate the dependence of the periodic shedding on communication between the

NOMENCLATURE

D	cylinder diameter	Vrms	vortex intensity perpendicular to the flow
θ	angle of the separator plate with the flow direction	v'v'	Reynolds normal stress in the direction perpendicular to the flow
ε	separator plate permeability	TKE	turbulence kinetic energy [$TKE = \frac{3}{4}\frac{(\overline{(u')^2}+\overline{(v')^2})}{U^2}$]
Re	Reynolds number [$Re = \frac{U_\infty . D}{\vartheta}$]	Urms	flowwise vortex intensity
ls*	nondimensionalized splitter plate length	u'	velocity change in flow direction
lg*	distance between dimensionless splitter plate and cylinder	v'	velocity change perpendicular to flow direction
lg**	distance between non-dimensionalized splitter plate rotation axis and cylinder	g	gravitational acceleration
U	flow velocity	hw	free water height
ϑ	kinematic viscosity of the fluid	fr	Froude number [$Fr = \frac{U_\infty .}{\sqrt{(g.h_w)}}$]
ρ	fluid density	u'u'	Reynolds normal stress in flow direction
u'v'	Reynolds shear stress		

of the periodic shedding on communication between the free vortex layers. He demonstrated that when splitter plate length (L) reached 5D (D is diameter of the cylinder), vortex shedding completely eliminated and pressure drag is reduced.

Cimbala and Chen (1994) experimentally performed for 60,000<Re<500,000 on a freely rotatable cylinder with fixed splitter plate length between 0.125≤L/D≤4 for comparing splitter plate equilibrium angle for subcritical, transitional, and supercritical Reynolds numbers. Shukla et al. (2009) studied for equilibrium angles of a rotatable splitter plate hinged on fixed cylinder with 0.75≤L/D≤ 7 and 1000<Re<10,000. They found that for L/D≤ 3, the oscillations appear to be periodic with a tip amplitude of 0.45D, and for higher L/D ratios, the non-periodic oscillations were observed. Shukla (2023) also work on the effect of attached flexible splitter plates with different lengths and stiffness on the flow field around a cylinder. Hence, freely rotatable splitter plates were commonly studied with different ratios of L/D and various range of Re numbers, and the effect of the length of splitter plate were presented (Cardell, 1993; Gu et al., 2012; Lee & You, 2013; Assi & Bearman, 2015; Lu et al., 2016; Teksin & Yayla, 2016).

The detached splitter plate was chosen as well to control the downstream flow structure of the bluff body. A splitter plate downstream of cylinder (Hwang et al., 2003), two splitter plates upstream of cylinder (Hwang & Yang, 2007), and a flexible splitter plate both upstream and downstream of cylinder (Wu et al., 2014) were applied to minimize disadvantages of the flow separation. Also, the thickness and the length of the splitter plate were studied to understand its effect on the wake flow. For Re=5000, Akilli et al. (2005) revealed that the thickness of the splitter plate has positively had the flow control when the gap length was equal or lower than 2D of the control cylinder. Kwon and Choi (1996) found out that the splitter plate length (L) was larger than a critical value that would yield to prevent the vortex shedding downstream of the cylinder. To minimize the drag coefficient, they presented an optimum splitter length which is between 1<L/D <2.

In addition to single splitter plates, Khairy (2008) compared three different model configurations: plane cylinder, cylinder with a splitter plate and a pair of splitter plates on each side of the cylinder's axis. The maximum drag reduction was observed 53% for two splitter plate configuration, and L/D ratio was equal to unity. Bao and Tao (2013) numerically investigated the wake control of a circular cylinder by dual plates symmetrically attached to the rear surface within the laminar flow regime (Re=20-160). They changed the angle of splitter plates to increase the drag reduction. Zhu et al. (2023) work on the effects of bilateral splitter plates located on different downstream positions and inclination angles on the flow structures around a circular cylinder at Re=100.

In his study, Ozgoren (2006) examined the flow in the square and circular cylinder wake region in the range of 550 ⩽ Re ⩽ 3400. He detected the changes in Strouhal numbers depending on the sections and section placement and showed their compatibility with the values in the literature. As expected, it was stated that the distance of vortex formation decreased with the increase of Reynolds number. In another study, Ozgoren and his colleagues (Ozgoren et al., 2011) examined the flow characteristics in the wake region of the cylinder and sphere at Re = 5000 and Re = 10000. They stated that small-scale vortices are more dominant in the sphere wake region and, unlike the cylinder, the highest value of TKE is seen at two points along the separation plates for the sphere due to the 3D flow. Eydi et al. (n.d) made a comparative analysis of different type of splitter plates. Sahin et al. (2021) made a series of experiment on the effect of gap between splitter plate and cylinder. Maruai et al. (2023) simulated on the effect of different splitter plate lengths on the flow induced vibration on a square cylinder.

In this study, even though perforated (Matsumoto et al., 2008) or permeable (Ozkan et al., 2017) splitter plates were used for a control element, we believe that the literature for perforated designed splitter plates have not been investigated thoroughly. This study innovates by systematically investigating the effects of varying permeability values downstream of a circular cylinder alongside different splitter plate lengths using PIV.

Maintaining a fixed gap ratio (G/D=1) between the splitter plates' leading edge and the cylinder surface, experiments were conducted at a Reynolds number of 5000 based on the cylinder diameter (D). The range of permeability values (∈=0.30, 0.50, 0.70) and splitter plate lengths (L/D=1, 2, 3) offers comprehensive data on their independent and combined influences on flow control. This approach not only enhances understanding of flow dynamics but also provides insights into optimizing configurations for effective flow manipulation in engineering applications. The use of PIV ensures high-resolution flow measurement, reinforcing the study's contribution to advancing experimental methodologies in fluid dynamics research.

2. MATERIALS AND METHODS

The experimental study took place at Cukurova University's Mechanical Engineering Department Fluid Mechanics Laboratory. A plexiglass cylinder, with dimensions of 0.06 m in diameter (D) and 0.45 m in height (h), was fabricated to serve as the baseline cylinder for investigating wake flow behavior in a vertically oriented configuration.

A perforated splitter plate, located at various downstream locations, is used to control the wake flow behavior. Perforated splitter plates were manufactured from nickel steel sheet having a thickness of $t=1\times10^{-3}$ m (Fig. 3). The hole diameter, d, was 2.5×10^{-3} m on the plate fabricated laser cutting machine. The length of the plates was 0.06 m, and the height of the plates were 0.45 m having same dimensions with the cylinder. Three distinct splitter plate permeabilities were investigated: ∈ = 0.3, 0.5, and 0.7. Permeability is defined as the ratio of the total hole area to the entire area of the splitter geometry. All variables are normalized by dividing by the cylinder diameter, D, and are indicated with the * index. The splitter plates were positioned downstream and aligned in the streamwise direction, with the gap between the leading

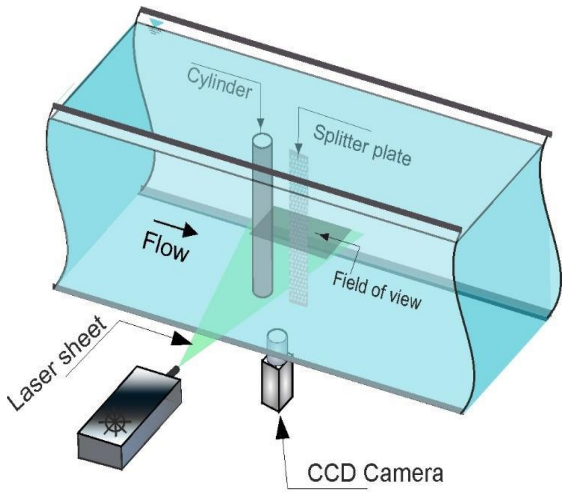

Fig. 1 A sketch of the experimental apparatus

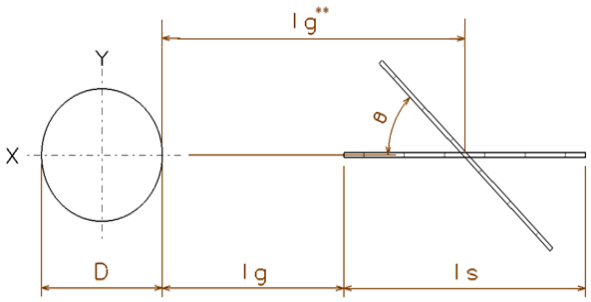

Fig. 2 A schematic diagram of the cylinder with perforated plate and examined parameters

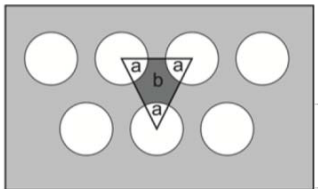

$$\varepsilon = \frac{A_{\text{total hole area}}}{A_{\text{total plate area}}}$$

$$\varepsilon = \frac{3a}{3a+b}$$

Fig. 3 Plate permeability definition

edge of the splitter plates and the cylinder surface (lg*) maintained at a constant lg* = 1 throughout the experiments. The length of the splitter plate, normalized by the cylinder diameter (D), was investigated at three different length ratios: ls* = 1, ls* = 2, and ls* = 3. In Fig. 1 and Fig. 2, the schematic experimental set-up system and geometrical dimensional representations of the cylinder and splitter plates are given.

$$ls^* = \frac{ls}{D} \tag{1}$$

$$lg^* = \frac{lg}{D} \tag{2}$$

$$lg^{**} = lg^* + ls^*/2 \tag{3}$$

Flows with subcritical Reynolds numbers, such as the Reynolds number chosen in this study (Re = 5000), are not in a stable regime due to the effect of adverse pressure gradients and the transition to turbulence. In subcritical flows, unsteady flow structures around the blunt body cause many uncertainties in terms of engineering and should be examined carefully. Adapting low Reynolds numbers to real-world flow structures requires maintaining geometric, kinematic and dynamic similarities between the experimental setup and the real system. Geometric similarity ensures that the scaled experimental setup accurately represents the physical geometry of the real-world application. Kinematic similarity focuses on matching flow velocities and accelerations between the model and the real system. Dynamic similarity ensures that the forces acting on the model are proportional to the forces in the actual application, thus preserving the overall flow behavior

$$Re = \frac{U_\infty . D}{\vartheta} \tag{4}$$

In equation number 4, Re is the Reynolds number, U_∞ =0.0837m/s free flow velocity, D is the cylinder diameter, ϑ=1.00401E-06 is the kinematic viscosity of

water at 20 ℃. All experiments were conducted in a water channel with a cross-sectional area of 0.75 m x 1 m, and the water height was maintained consistently at 0.5 m.

In this study, PIV technique was employed to measure the velocity vector fields. PIV works by capturing two sequential images of a flow seeded with tracer particles. By using cross-correlation techniques, the displacement of these particles between the images is determined. This displacement, along with the known time interval between the images, enables the calculation of velocity vectors at discrete points within the flow field. Vorticity, which measures the local rotation of fluid elements, is derived from the velocity field as the curl of the velocity. In two-dimensional (2D) flows, vorticity is calculated by equation 5 and shear stress tensor by equation 6. For estimating required derivatives form PIV data, finite difference methods are used (i.e. equation 7 and equation 8)

$$\omega = \frac{\partial \mathrm{v}}{\partial \mathrm{x}} - \frac{\partial \mathrm{u}}{\partial \mathrm{y}} \tag{5}$$

$$\tau_{xy} = \mu\left(\frac{\partial \mathrm{v}}{\partial \mathrm{x}} + \frac{\partial \mathrm{u}}{\partial \mathrm{y}}\right) \tag{6}$$

$$\frac{\partial \mathrm{v}}{\partial \mathrm{x}} \approx \frac{v_{i+1,j} - v_{i-1,j}}{2\Delta x} \tag{7}$$

$$\frac{\partial \mathrm{u}}{\partial \mathrm{y}} \approx \frac{u_{i,j+1} - u_{i,j-1}}{2\Delta y} \tag{8}$$

Due to the large amount of data, the measurements were carried out using the Dantec Dynamics PIV system and processed with the Flow Manager software installed on the computer. The wake flow behavior was examined using a Dantec PIV system equipped with two Nd: YAG pulsed laser sources emitting light at a wavelength of 532 nm. Each laser had a maximum energy output of 120 mJ for illuminating the flow field. A 2 mm thick laser sheet, oriented parallel to the bottom surface of the water channel and intersecting the mid-plane of the cylinder, was used for illumination. The water was seeded with neutrally buoyant spherical particles measuring 12 μm in diameter.

A CCD camera fitted with a Nikon AF micro 60 f/2.8D lens was employed to capture images at a resolution of 1600x1200 pixels and a focal length of 60 mm. The physical field of view size was approximately 3.8 times the cylinder diameter (3.8D) by 2.8 times the cylinder diameter (2.8D). PIV measurements were conducted at a sampling frequency of 15 Hz, with 1000 image pairs collected for each test case. Image processing utilized rectangular effective interrogation windows of size 32x32 pixels.

During the query process, an overlap of 50% was used to meet the Nyguist criterion. Westerweel (1993), Adrian (1991) and Raffel et al. (2007) explained the mathematical and physical approaches used in the PIV method in detail in their studies. Westerweel (1993) calculated that in the PIV method, there is an uncertainty of approximately 2% in the velocity measurements of the particles due to reasons such as the random distribution of the particles to be illuminated by the laser, the size of the area where the velocity calculations are made, and the sensitivity of the measurement and imaging devices. Since a similar approach was used in this study, the uncertainty in speed was accepted as approximately 2% compared to the depth-averaged speed in the experiments. Finally, turbulent statistics such as turbulent kinetic energy, Reynolds shear stress and so forth were calculated for each test case. The Stokes number of the particles was calculated to be around 1.83x10-3, and this value shows that the particles follow the flow lines exactly in the experiments (Raffel et al., 2007; Gozmen et al., 2013). The Froude number for the open-top rectangular section water channel used is given in equation 9.

$$Fr = \frac{U_{\infty}.}{\sqrt{(g.h_w)}} \tag{9}$$

According to Eq. 9, the Froude number was calculated as 0.042, and since the critical Froude number was much lower than (1), the effect of the flow free surface was ignored.

3. RESULTS AND DISCUSSIONS

TKE profiles at different downstream locations for different permeabilities and plate lengths are given in Fig. 4 and Fig. 5. In these figures, each column presents different plate lengths (i.e., L/D= 1, 2, and 3) and each line shows the nondimensional position of the cross-section from which the data is taken in the wake flow region, according to the cylinder diameter (i.e., x/D = 0.5, 1, 1.5, 2, 2.5, and 3). In each cell, TKE profiles for different permeabilities were given and compared with baseline cylinder. The profiles look identical with similar characteristic peaks at the shear layer of the cylinder in which peak points represent the highest value of TKE.

As large-scale vortex shedding causes fluctuations at further downstream of the cylinder, it can be seen that TKE levels increase in both the shear layers and the wake region with increasing regions downstream of the cylinder. For L/D≥2, splitter plates' effect can be observed from the beginning of the section from x/D=0.5 for all permeabilities, and as the section distance increases, the effect of the plate became more obvious because of the vortex shedding fluctuations. Since the perforated splitter plate prevents the interaction of the emanated shear layers from the cylinder's upper and lower points, the effect of the perforated separating plate increases as the plate length increases. As a result, this reduces downstream and transverse fluctuations, and a stabilized wake flow occurs downstream of the cylinder.

At high Reynolds numbers, turbulence formations occur in the wake region due to periodic changes in pressure and velocity distribution. In other words, in the flow in this region, the speed and flow direction of the fluid constantly changes. Dimensionless TKE is a measure of the intensity of turbulence and can be used as an evaluation indicator for flow properties in the wake region as stated by Chen and Pinar (Chen et al., 2014; Pinar et al., 2015).

The TKE is typically given by the formula:

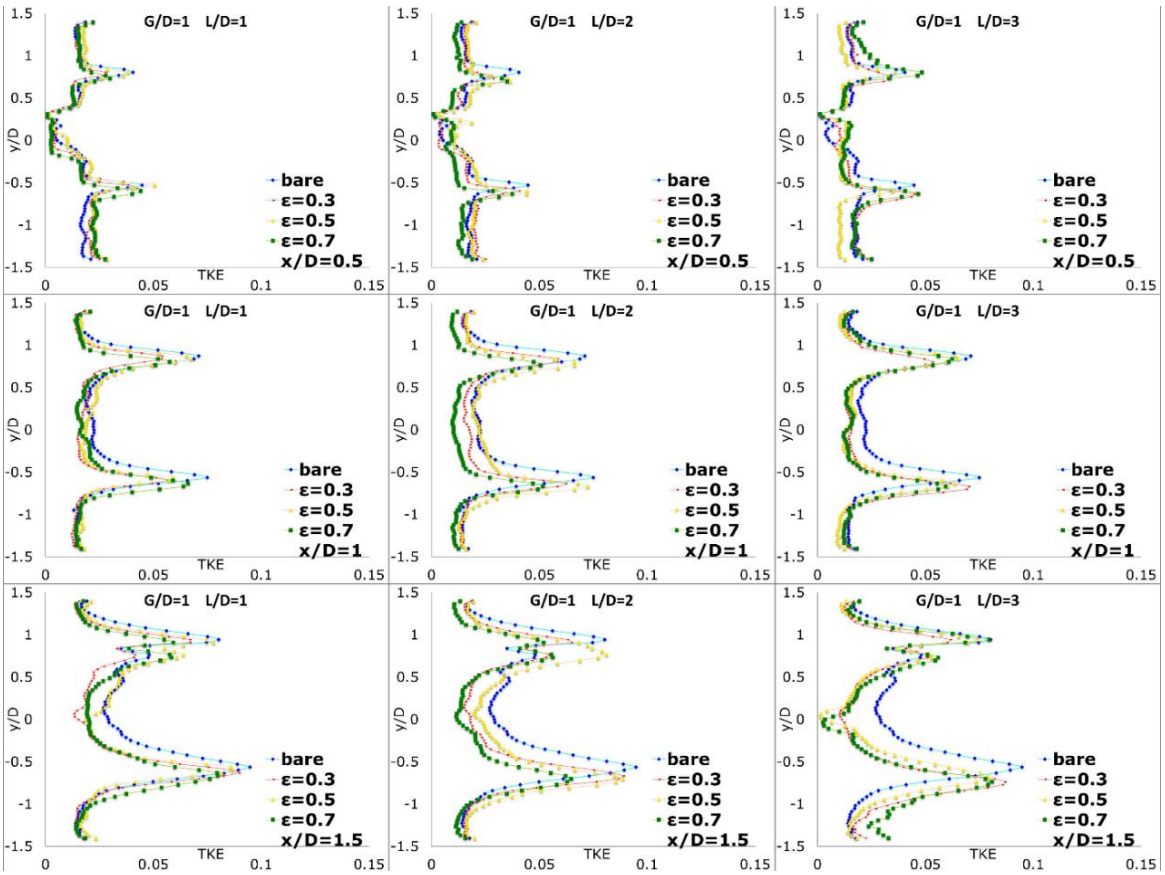

Fig. 4 Profiles of TKE at 0.5 ≤ x / D ≤1.5 for different permeabilities and length ratios

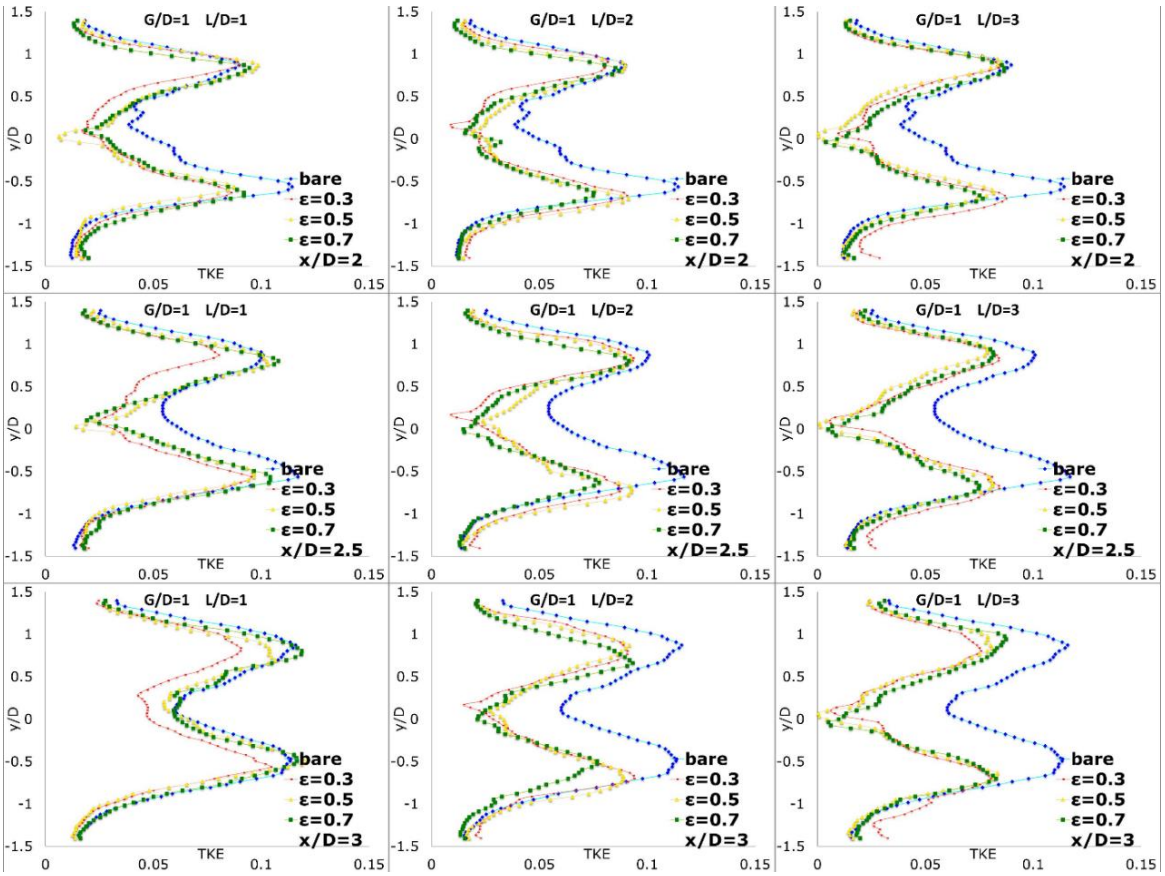

Fig. 5 Profiles of TKE at 2 ≤ x / D ≤3 for different permeabilities and length ratios

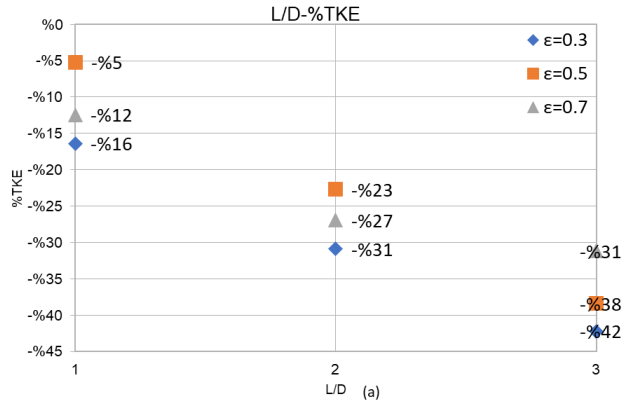

Fig. 6 Max TKE values

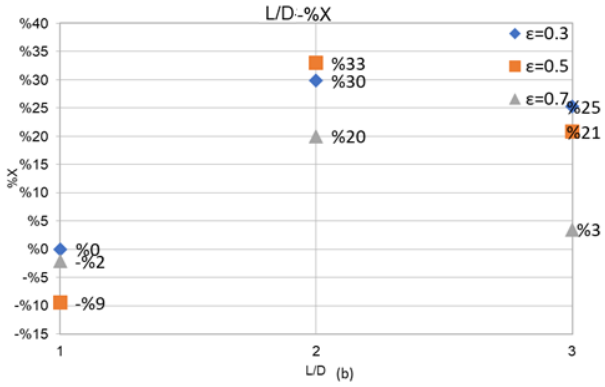

Fig. 7 Max TKE formation points

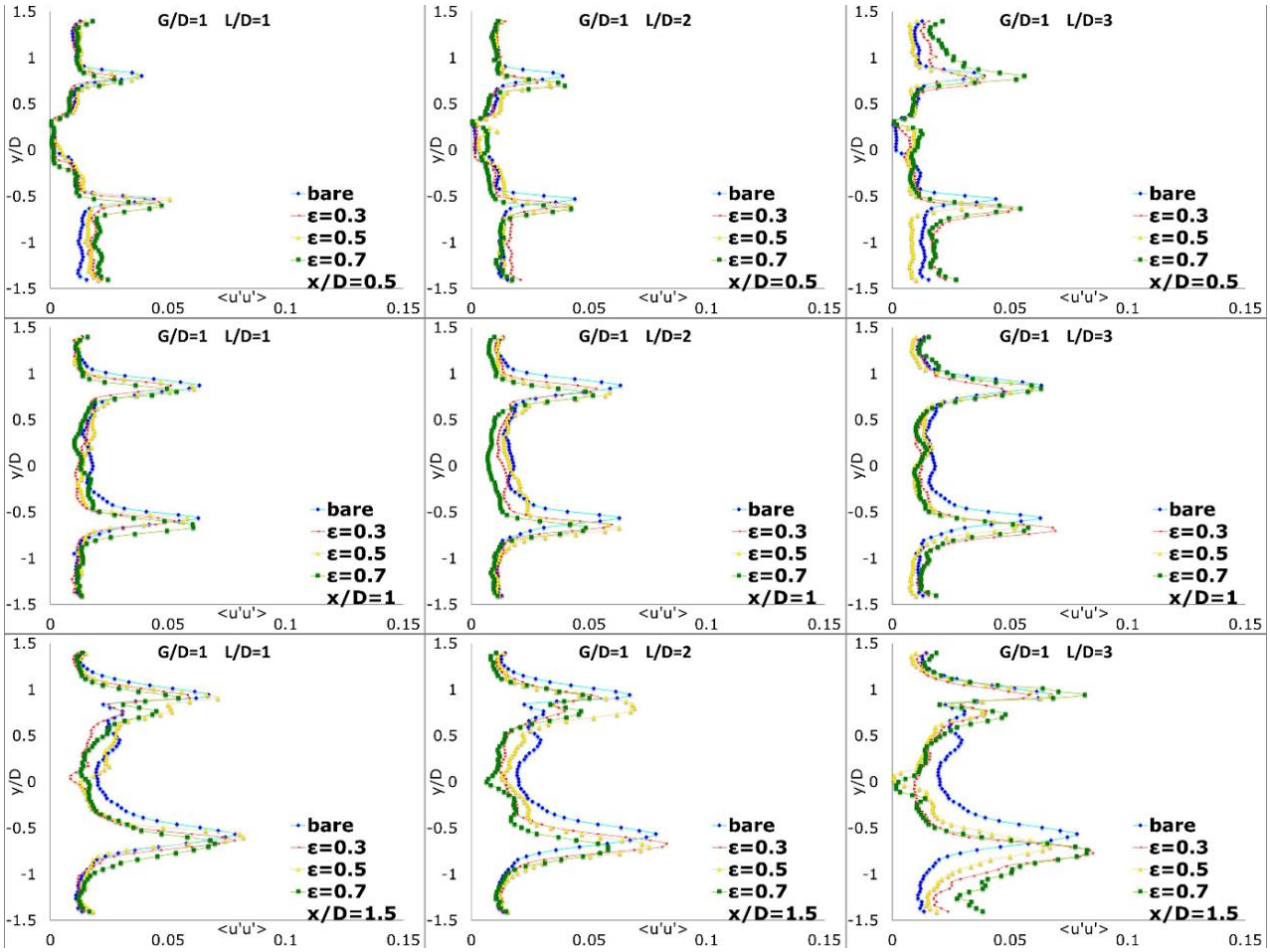

Fig. 8 Profiles of streamwise Reynolds stress at 0.5 ≤ x / D ≤1.5 for different permeabilities and length ratios

$$TKE = \frac{1}{2}\left(\overline{(u')^2} + \overline{(v')^2} + \overline{(w')^2}\right) \quad (10)$$

For 2D flow, (Sheng et al., 2000; Ozkan et al., 2017) velocity component in z direction, w', is neglectable and factor will be ¾ for adjust the scaling of the kinetic energy. Average TKE formula will be:

$$TKE = \frac{3}{4}\frac{\left(\overline{(u')^2} + \overline{(v')^2}\right)}{U^2} \quad (11)$$

We represented change of the peak values of TKE and the corresponding downstream positions due to bare cylinder TKE values in Fig. 6 and Fig. 7. The length of splitter plate, L/D =1, 2, and 3, were shown as parameter for three different permeabilities to understand how perforated plate would affect the maximum TKE value, and it also provides further downstream positions for various L/D values. Hence, at first glance, we would say that all splitter plate configurations yield to decrease the maximum TKE from 5% to 42% compared to bare splitter plate. The peak magnitude's location of maximum TKE

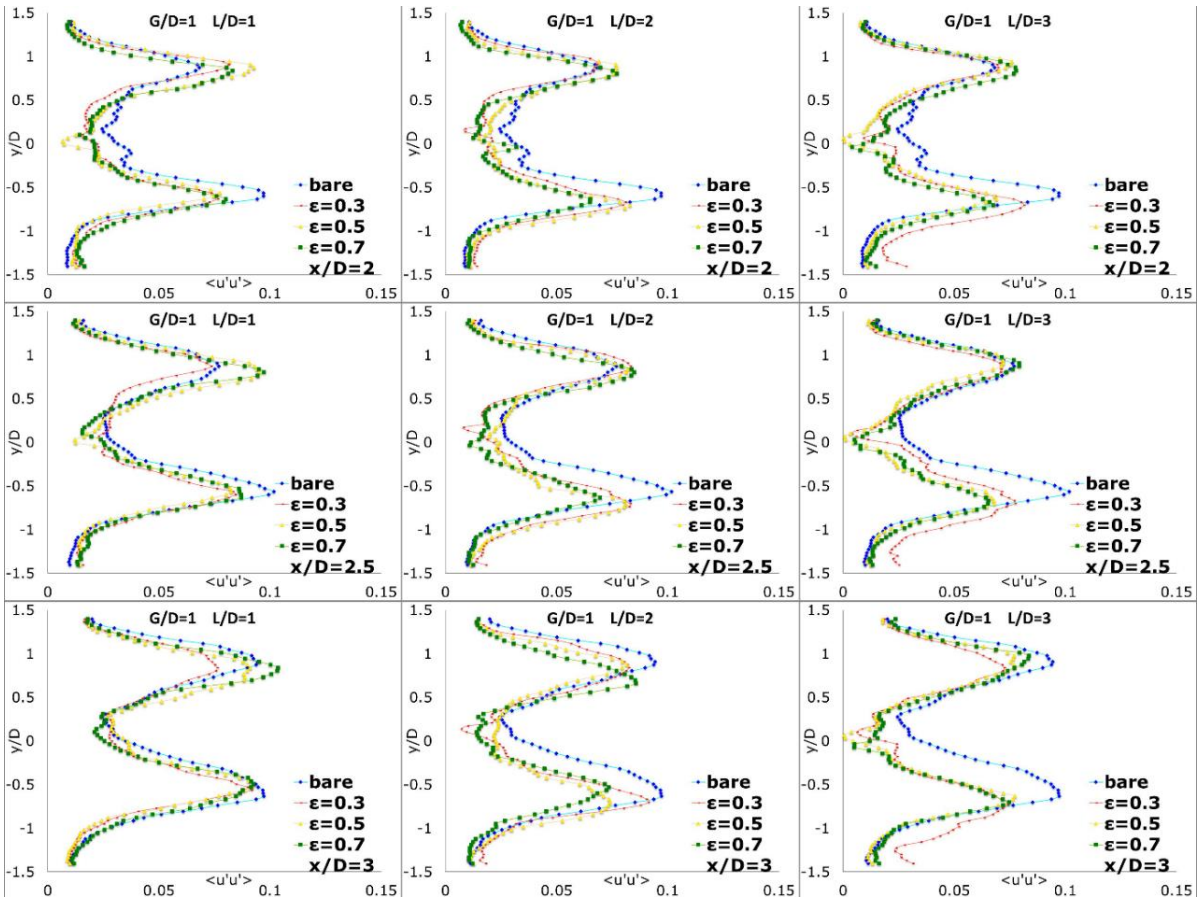

Fig. 9 Profiles of streamwise Reynolds stress at 2 ≤ x / D ≤3 for different permeabilities and length ratios

moves 33% higher than bare case. For the permeability of ε=0.5, we only observed the peak location closer to the cylinder at L/D =1, therefore, except this case, we would observe that the perforated splitter plates would efficiently work to control the flow shedding by reducing the TKE. At L/D =3, we can observe that the maximum TKE reduction percentages for all permeability values. Even though peak positions would be different from each other, maximum TKE decreases which is 42% would be observed at L/D =3 for ε=0.3, and it has 25% movement further downstream of peak location.

Increasing the permeability would cause to decrease the effectiveness of the flow control as in ε=0.7, the peak magnitude is only to move 3% further because its structural unity goes to annihilation for higher permeabilities. However, we would see that the promising decrease in TKE by using perforated splitter plates for all downstream values of L/D.

Profiles of streamwise Reynolds Stress, |u'u'|, at different downstream locations for different permeabilities and plate lengths are given in Fig. 8 and Fig. 9. In the figures, each column presents different plate lengths, and each line shows the nondimensional position of the cross-section from which the data is taken in the wake flow region, according to the cylinder diameter (i.e., x/D = 0.5, 1, 1.5, 2, 2.5, and 3). In each cell of |u'u'| profile, different permeabilities were given with baseline cylinder data. Profiles look identical with similar characteristic peaks in the shear layer of the cylinder in which the peak data represent the highest value of |u'u'| since the shear layers lead to large velocity gradient. As can be seen, peeks grow as the location of x/D shifts towards downstream direction due to the vortex shedding and wake vortex intensification. Compared to the baseline cylinder, the perforated plates have insignificant effect on |u'u'| magnitudes in the shear layer prior to x/D=2 but at x/D=2, the certain amount of reduction of |u'u'| would be observed. For all permeabilities, the magnitudes of |u'u'| in the wake region are reduced at further downstream regions.

Figures 10 and 11 illustrate profiles of transverse Reynolds Stress, |v'v'| at different downstream locations for different permeabilities and plate lengths. In these figures, each column presents different plate lengths, and each line shows the nondimensional position of the cross-section from which the data is taken in the wake flow region, according to the cylinder diameter (i.e., x/D = 0.5, 1, 1.5, 2, 2.5, and 3). The values of |v'v'| grow as the location of x/D shifts towards downstream direction due to vortex shedding and wake vortex intensification and highest value of |v'v'| occurs in the shear layers because of velocity gradients. It is clearly seen that both the permeability and length ratio of the splitter plate are effective on the certain reduction of |v'v'| and by the x/D=1.5 station, |v'v'| profiles for all permeabilities and plate length ratio L/D ≥2 clearly separated from the baseline |v'v'| profile. It is also noted that for plate permeability of ε = 0.3, it is more effective at x/D≥1.5 due to increased blockage of shear layer interactions.

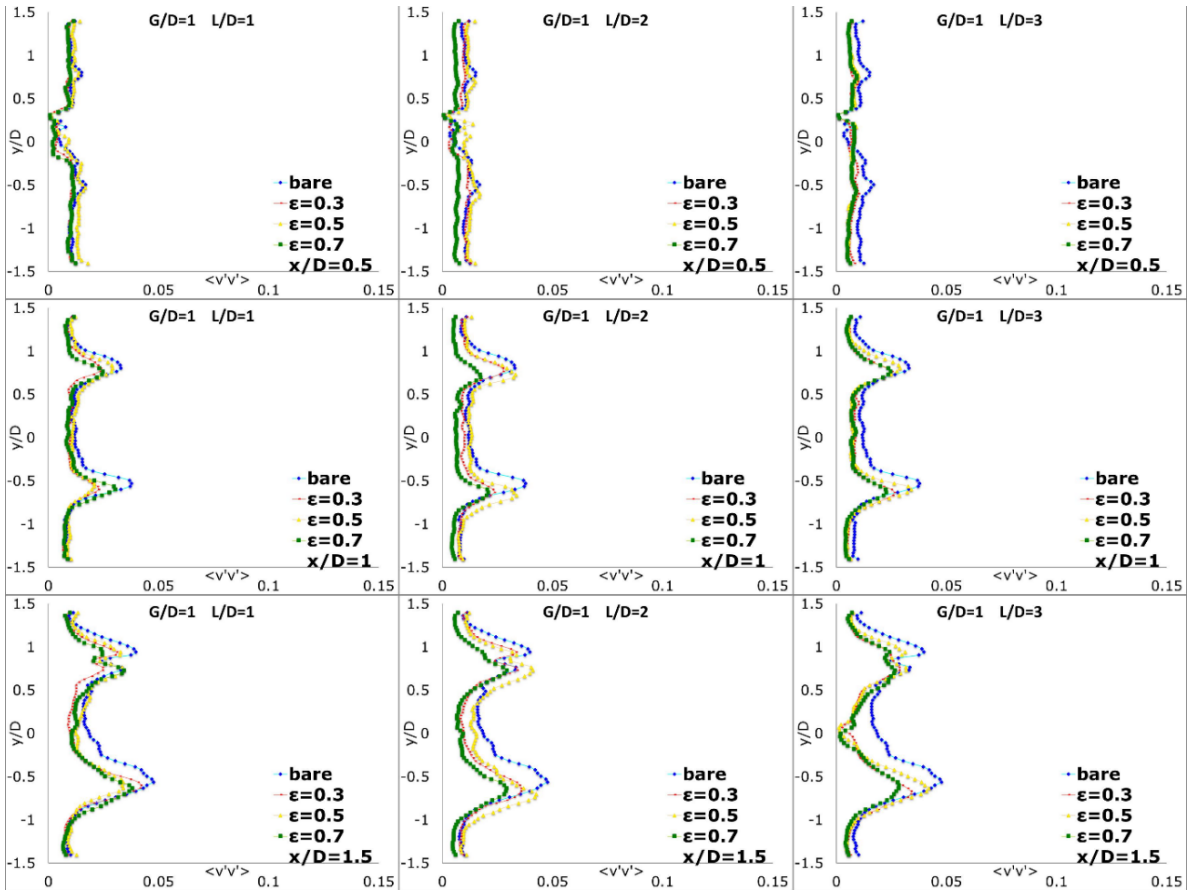

Fig. 10 Profiles of transverse Reynolds stress at 0.5 ≤ x / D ≤1.5 for different permeabilities and length ratios

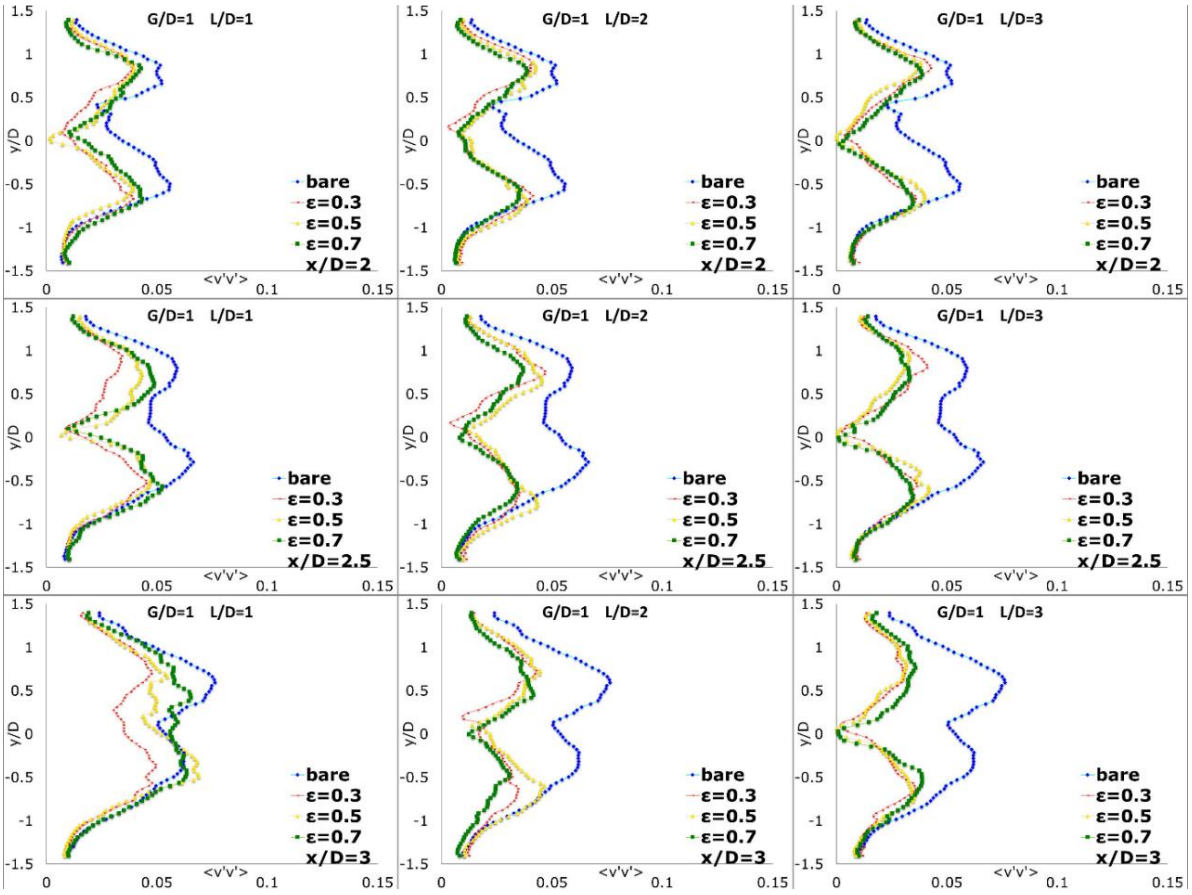

Fig. 11 Profiles of transverse Reynolds stress at 2 ≤ x / D ≤3 for different permeabilities and length ratios

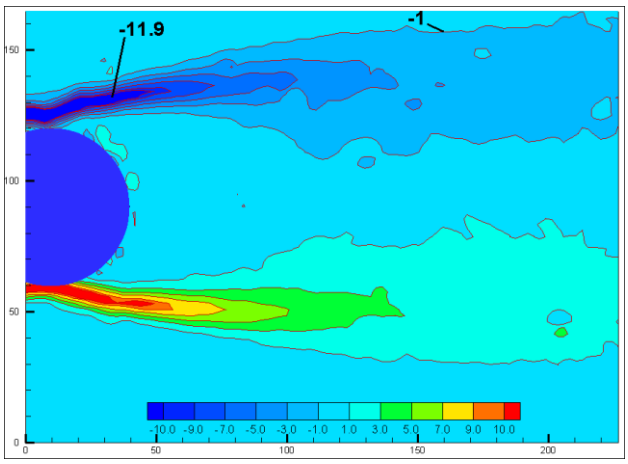

Fig. 12 Vorticity distribution for base cylinder

For all cases, time averaged normalized vortex distribution in the downstream area is given in Figs. 12 , 13, 14 and 15. Vortex magnitudes with a negative sign indicate clockwise rotation. For the base case, shear layers are formed on both sides of the cylinder and their strength is further reduced in the downstream direction. The magnitude of the vortex reaches -11.9 1/s in the shear layer. For L/D =1 case, maximum vortex value is reduced by %1, %1 and %55 for ε=0.3, 0.5 and 0.7 in order.

It is obvious that shear layer strength is reduced due to base cylinder case because the perforated splitter in the wake region prevents interactions of shear layers. Splitter plate effectiveness is increased with the increasing permeability. In all cases, strength of vorticities decreased as the splitter plate length increased and effect of the permeability on vorticity strength varies with length of the splitter plate. For L/D =2 case, max vortex value is reduced by %2, %1 and %13 for ε=0.3, 0.5 and 0.7 respectively. For L/D =3 case, max vortex value is reduced by %14, %11 and %18 for ε=0.3, 0.5 and 0.7 respectively. As anticipated of this study, the shear layers of the cylinder extend along flow direction when the splitter plate length increase compared to the base cylinder.

Change of the peak magnitude of Reynolds shear stress with length is given in Fig. 16 for all test cases. Investigations conducted by Gozmen et al. (2013) and Ozkan et al. (2017) on splitter plates have revealed that the mitigation of vortex shedding leads to a decrease in turbulence statistics, including turbulent kinetic energy and Reynolds shear stress, downstream of the cylinder. Furthermore, the assessment of Reynolds shear stress

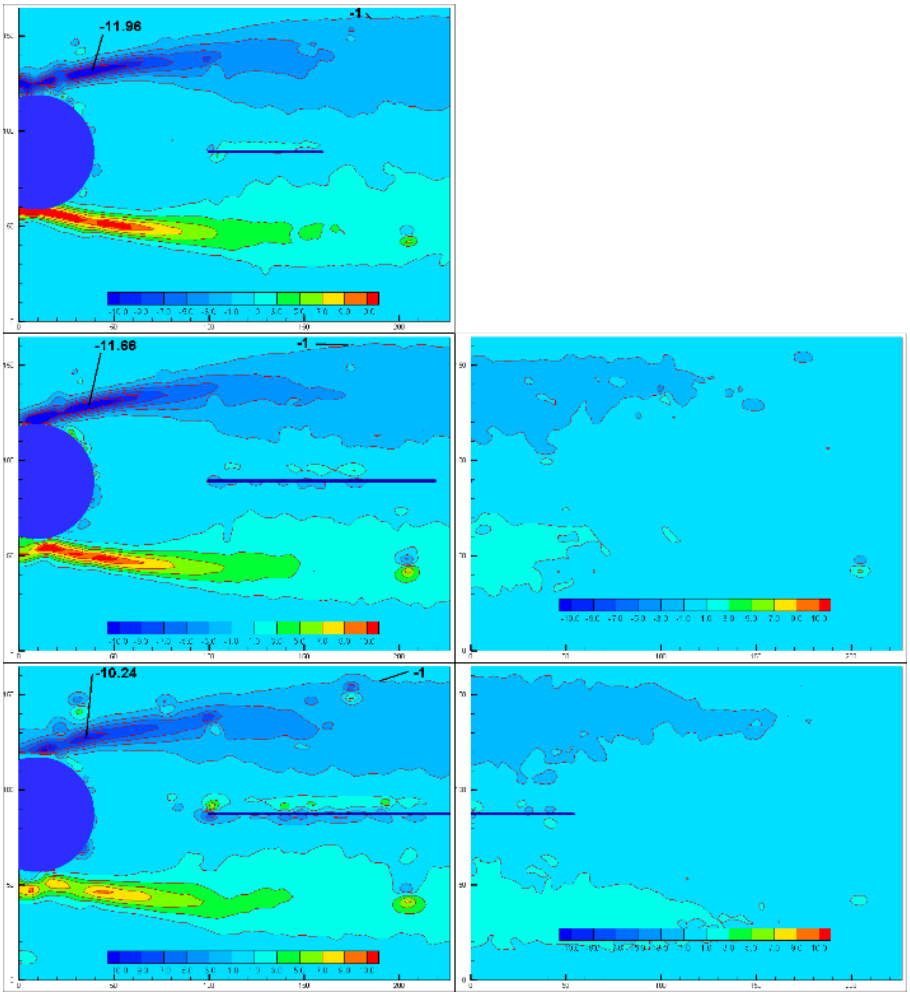

Fig. 13 Vorticity distributions for permeability value, ε, 0.3 (L/D values 1, 2 and 3 in rows)

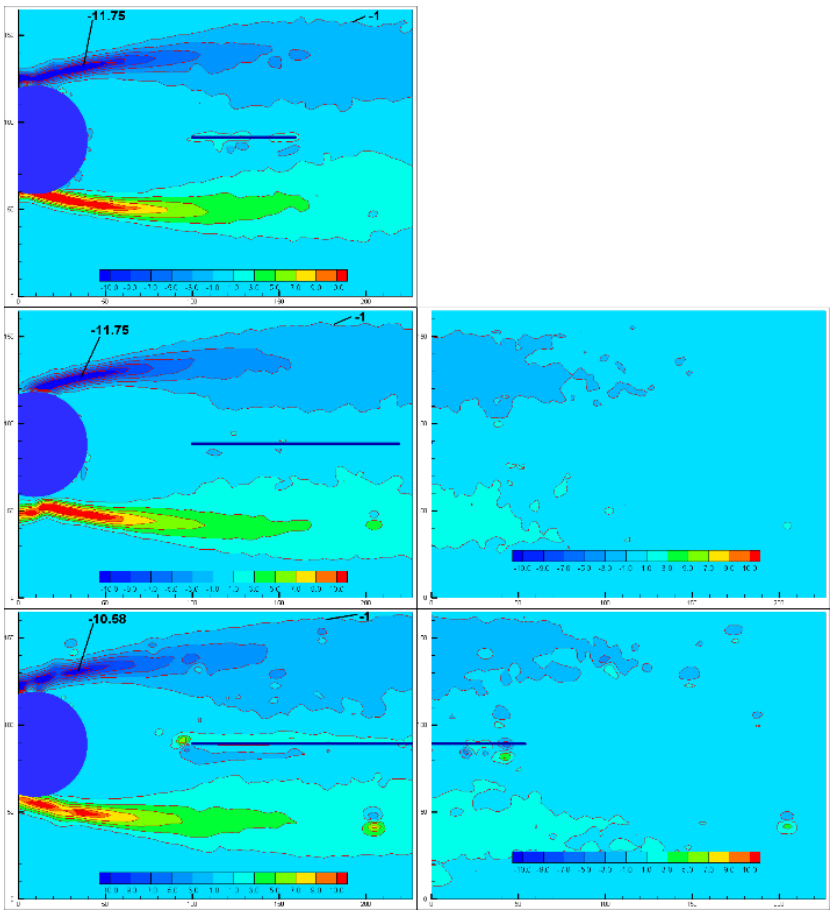

Fig. 14 Vorticity distributions for permeability value, e, 0.5 (L/D values 1, 2 and 3 in rows)

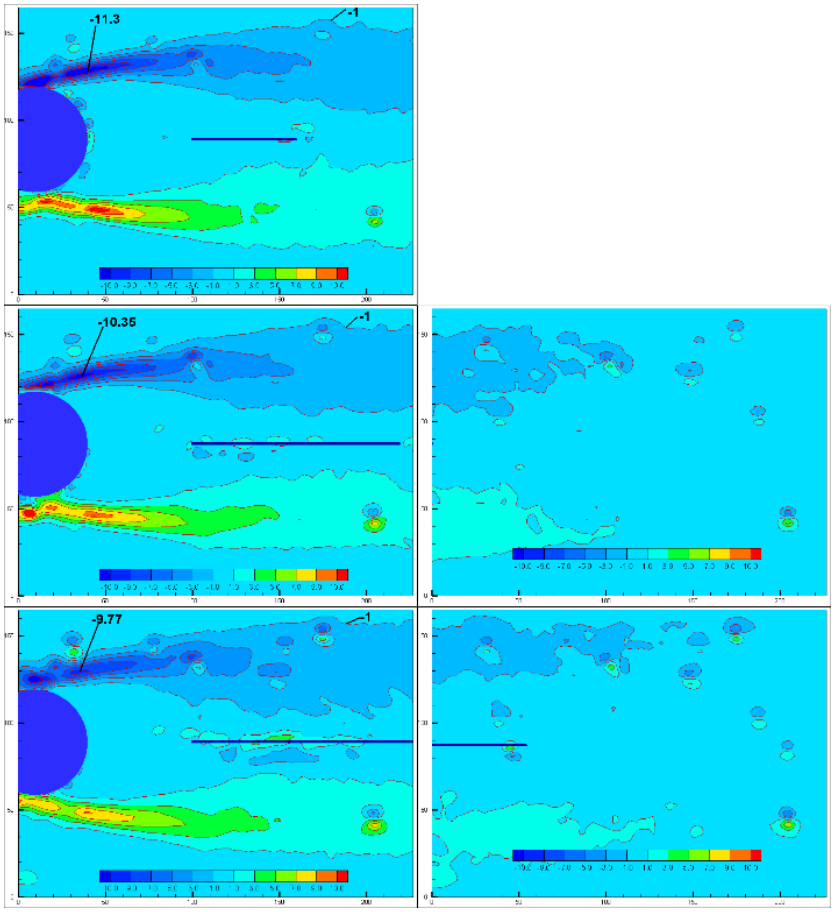

Fig. 15 Vorticity distributions for permeability value, e, 0.7 (L/D values 1, 2 and 3 in rows)

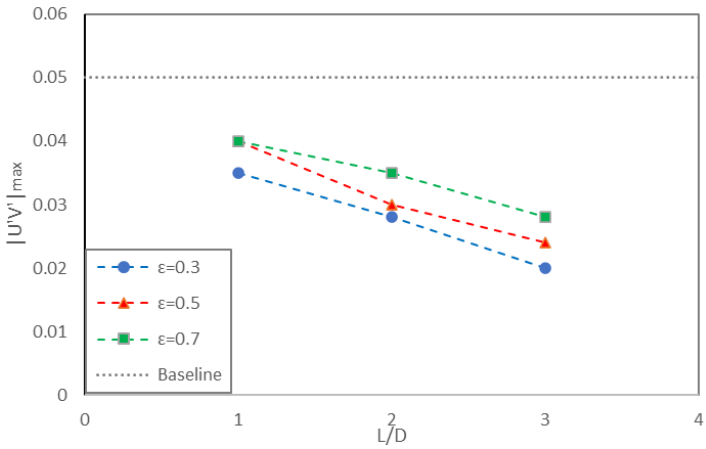

Fig. 16 Variation of the peak magnitude of Reynolds shear stress with length ratio for all test cases

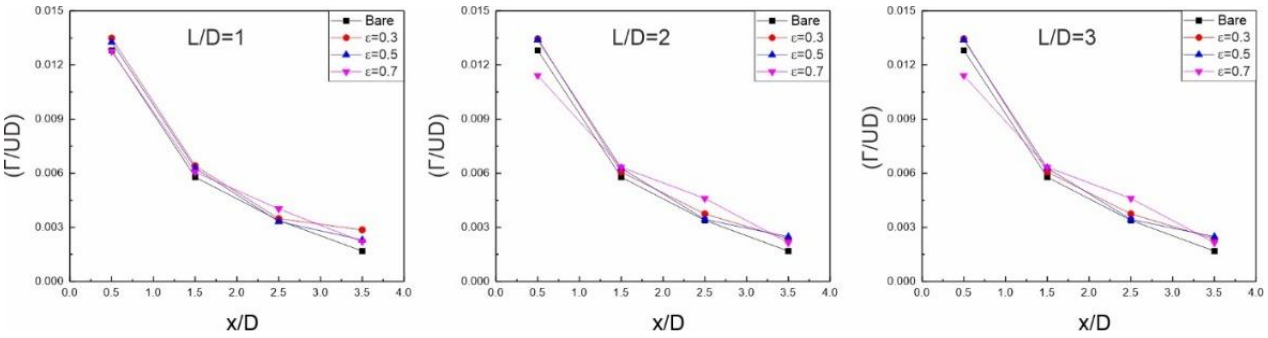

Fig. 17 Variation of maximum circulation in the shear layer through downstream

holds significance as it provides valuable insights into velocity fluctuations within the wake region (Gao et al., 2020). The peak magnitude of Reynolds shear stress is found as 0.05 for baseline cylinder. For the splitter plate length of L/D=1, the peak value of Reynolds shear stress is diminished up to 30% for ε = 0.3, 20% for ε = 0.5, and 20% for ε = 0.7. For the splitter plate length of L/D=2, the peak value of Reynolds shear stress is diminished up to %44 for ε = 0.3, %40 for ε = 0.5 and %30 for ε = 0.7. For the splitter plate length of L/D=3, the peak value of Reynolds shear stress decreased down to %60 for ε = 0.3, %52 for ε = 0.5 and %44 for ε = 0.7. As seen from the results, with increasing permeability, blockage of the shear layer decreases. Ozkan et al. (2017) also noted the similar behavior in their studies. The decrease in Reynolds shear stress can also be interpreted as a reduction in the drag coefficient of the cylinder. This relationship was demonstrated by Ozkan et al. (2017), who found that a decrease in turbulent statistics correlates with a reduction in the drag coefficient compared to the baseline cylinder.

The circulation can be calculated based on the vortex using following expression

$$\boldsymbol{\Gamma} = \iint \boldsymbol{\omega_z dxdy} \tag{12}$$

In this sense, time averaged circulation in the flow field is approximately zero since vortex structure of cylinder with or without splitter plate is nearly symmetrical with respect to wake centerline of the cylinder. On the other hand, the variation of circulation through the shear layer can be evaluated to obtain information about vortex strength. Figure 1 presents variation of normalized maximum circulation in the sear layer of the cylinder through downstream. It is obtained that the highest circulation is evaluated at x/D=0.5 for all cases. The magnitude of circulation decreases with increasing downstream location. At x/D=3.5, the magnitude of circulation of bare cylinder is lower than cases of splitter plate since plate causes elongation of the shear layers through downstream. Therefore, it can be concluded that the variation of circulation exhibits a similar trend to the changing vorticity magnitude of the shear layer. The circulation serves as a quantitative measure of the strength of the vortex, with higher circulation values indicating a more powerful and influential vortex in the flow field.

4. CONCLUSION

A series of experiments were performed at Re=5x10^3 to define the effect of splitter plates with different permeabilities on flow structures in the wake region of a bare cylinder. The splitter plates with different permeabilities (ε = 0.3, 0.5 and 0.7) and different length ratios (L/D =1, 2 and 3) located in the wake centerline of the cylinder (G/D=1). Flow structure and turbulence statistics evaluated by employing PIV measurements. For this purpose, the peak value of turbulent kinetic energy, formation point of peak values of turbulent kinetic energy and magnitude of Reynolds shear stress were compared to

bare cylinder case. Evaluated results using PIV measurements indicated as below:

- Permeability and length of the plate are effective parameters to reduce vortex shedding. As splitter plate length increased, turbulent kinetic energy reduced in all situations. Also, formation distance of peak value of TKE in the flow direction increased nearly in all situations except L/D=1, ε =0.50 and 0.70 situations.
- Vortex formation can be delayed with the increasing the splitter plate length. Flow control is achieved for the gap L/D=3 and ε=0.3. The peak magnitude of turbulence kinetic energy is reduced up to 42%.
- For overall results, maximum reduction in peak magnitude of Reynolds shear stress is also achieved for ε=0.3 and L/D=3 as compared to the base cylinder.

CONFLICT OF INTEREST

No conflicts to disclose.

AUTHORS CONTRIBUTION

Serdar Şahin: Conceptualization, Formal analysis, Investigation, Methodology, Validation, Visualization, Writing – original draft, Writing – review & editing. **Tahir Durhasan:** Investigation, Writing – review & editing**. Engin Pınar:** Writing – review & editing. **Hüseyin Akıllı:** Conceptualization, Supervision

REFERENCES

Adrian, R. J. (1991). Particle-Imaging techniques for experimental fluid mechanics. *Annual Review of Fluid Mechanics*, *23*(1), 261-304. https://doi.org/https://doi.org/10.1146/annurev.fl.23.010191.001401

Akilli, H., Sahin, B., & Tumen, N. F. (2005). Suppression of vortex shedding of circular cylinder in shallow water by a splitter plate. *Flow Measurement and Instrumentation*, (16), 211-219. https://doi.org/doi:10.1016/j.flowmeasinst.2005.04.004

Assi, G. R., & Bearman, P. W. (2015). Transverse galloping of circular cylinders fitted with solid and slotted splitter plates. *Journal ofFluidsandStructures*, (54), 263-280. https://doi.org/http://dx.doi.org/10.1016/j.jfluidstructs.2014.11.005

Bao, Y., & Tao, J. (2013). The passive control of wake flow behind a circular cylinder by parallel dual plates. *Journal of Fluids and Structures*, *37*, 201-219. https://doi.org/10.1016/j.jfluidstructs.2012.11.002

Blevins, R. D. (1985). The effect of sound on vortex shedding from cylinders. *Journal of Fluid Mechanics.* (161), 217-237. https://doi.org/https://doi.org/10.1017/S0022112085002890

Cardell, G. S. (1993). *Flow Past a Circular Cylinder with a Permeable Wake Splitter Plate* [*Phd Thesis*, California Institute of Technology]. Pasadena, California, USA:

Chen, W. L. (2013). Suppression of vortex-induced vibration of a circular cylinder using suction-based flow control. *Journal of Fluids and Structures*, *42*. https://doi.org/https://doi.org/10.1016/j.jfluidstructs.2013.05.009

Chen, W., Li, H., & Hu, H. (2014). An experimental study on a suction flow control method to reduce the unsteadiness of the wind loads acting on a circular cylinder. Experiments in Fluids, *54*. https://doi.org/https://doi.org/10.1007/s00348-014-1707-7

Cimbala, J. M., & Chen, K. T. (1994). Supercritical Reynolds number experiments on a freely rotatable cylinder/splitter plate body. *Physics of Fluids (1994-present)*, (6). https://doi.org/10.1063/1.868191

Eydi, F., Mojra, A., & Abdi, R. (n.d.). Comparative analysis of the flow control over a circular cylinder with detached flexible and rigid splitter plates. *Journal of Physics of Fluids*, (34). https://doi.org/https://doi.org/10.1063/5.0110398

Favier, J., Dauptain, A., Basso, D., & Bottaro, A. (2009). Passive separation control using a self-adaptive hairy coating. *Journal of Fluid Mechanics*, *627*, 451-483. https://doi.org/10.1017/S0022112009006119

Fujisawa, N., Kawaji, Y., & Ikemoto, K. (2001). Feedback control of vortex shedding from a circular cylinder by rotational oscillations. *Journal of Fluids and Structures*, (15), 23-37. https://doi.org/DOI:10.1006/jfls.2000.0323

Gao, D. L., G. B. C., Huang, Y. W., Chen, W. L., & Li, H. (2020). Flow characteristics of a fixed circular cylinder with an upstream splitter plate: On the plate-length sensitivity. *Experimental Thermal and Fluid Science*, (117). https://doi.org/https://doi.org/10.1016/j.expthermflusci.2020.110135

Gozmen, B., Akilli, H., & Sahin, B. (2013). Passive control of circular cylinder wake in shallow flow. *Measurement*, (46), 1125-1136. https://doi.org/http://dx.doi.org/10.1016/j.measurement.2012.11.008

Gu, F., J. S. Wangb., X. Q. Qiao., & Z. Huang. (2012). Pressure distribution, fluctuating forces and vortexs hedding behavior of circular cylinder with rotatable splitter plates. *Journal of Fluids and Structures*, 263-278. https://doi.org/doi:10.1016/j.jfluidstructs.2011.11.005

Guilmineau, P. Q. (2002). A numerical simulation of vortex shedding from an oscillating circular cylinder. *Journal of Fluids and Structures*, (16), 773-794. https://doi.org/https://doi.org/10.1006/jfls.2002.0449

Hwang, J. Y., & Yang, K. S. (2007). Drag reduction on a circular cylinder using dual detached splitter plates. *Journal of Wind Engineering and Industrial Aerodynamics*, (95), 551-564. https://doi.org/10.1016/j.jweia.2006.11.003

Hwang, J. Y., Yang, K. S., & Sun, S. H. (2003, August). Reduction of flow-induced forces on a circular cylinder using a detached splitter plate. *Physics of Fluids*, *15*(8), 2433-2436. https://doi.org/10.1063/1.1583733

Khairy, N. A. (2008). Evaluation of base shield plates effectiveness in reducing the drag of a rough circular cylinder in a cross flow. *Wind and Structures*, *11*(5), 377-389. https://doi.org/http://dx.doi.org/10.12989/was.2008.11.5.377

Kwon, K., & Choi, H. (1996). Control of laminar vortex shedding behind a circular cylinder using splitter plates. *Physics of Fluids-American Institute of Physics*, *8*(2). https://doi.org/10.1063/1.868801

Lecordier, J. C., Hamma, L., & Parantheon, P. (1991). The control vortex shedding behind heated cylinders at low Reynolds numbers. *Experiments in Fluids* (10), 224-229. https://doi.org/https://doi.org/10.1007/BF00190392

Lee, J., & You, D. (2013). Study of vortex-shedding-induced vibration of a flexible splitter plate behind a cylinder. *Physics of Fluids*, *25*(110811). https://doi.org/10.1063/1.4819346

Lu, L., Guo, X. L., Tang, G. Q., Liu, M. M., Chen, C. Q., & Xie, Z. H. (2016). Numerical investigation of flow-induced rotary oscillation of circular cylinder with rigid splitter plate. *Physics of Fluids*, (28). https://doi.org/doi: 10.1063/1.4962706

Maruai, N. M., Ali, M. S., Zaki, S. A., Ardila-Rey, J. A., & Ishak, I. A. (2023). The influence of different downstream plate length towards the flow-induced vibration on a square cylinder. *Scientific Reports*. https://doi.org/https://doi.org/10.1038/s41598-023-44388-w

Matsumoto, M., Hashimoto, M., Yagi, T., Nakase, T., & Maeta, K. (2008). *Steady galloping/unsteady galloping and vortex-induced vibration of bluff bodies associated with mitigation of karman vortex shedding*. BBAA VI International Colloquium on:Bluff Bodies Aerodynamics & Applications. Milano.

Ozgoren, M. (2006). Flow structure in the downstream of square and circular cylinders. *Flow Measurement and Instrumentation*, *17*(4), 225-235. https://doi.org/https://doi.org/10.1016/j.flowmeasinst.2005.11.005

Ozgoren, M., Pinar, E., Sahin, B., & Akilli, H. (2011). Comparison of flow structures in the downstream region of a cylinder and sphere. *International Journal of Heat and Fluid Flow*, (32), 1138-1146. https://doi.org/https://doi.org/10.1016/j.ijheatfluidflow.2011.08.003

Ozkan, G. M., Firat, E., & Akilli, H. (2017). Passive flow control in the near wake of a circular cylinder using attached permeable and inclined short plates. *Ocean Engineering*, (134), 35-49. https://doi.org/http://dx.doi.org/10.1016/j.oceaneng.2017.02.014

Özdil, N. F. (2013). *Investigation of flow characteristics around in-line horizontal cylinders in shallow waters* [PhD. Thesis, Adana: Cukurova University].

Pinar, E., Ozkan, G. M., Durhasan, T., Aksoy, M. M., & Huseyin Akilli, B. S. (2015). Flow structure around perforated cylinders in shallow water. *Journal of Fluids and Structures*, (55), 52-63. https://doi.org/https://doi.org/10.1016/j.jfluidstructs.2015.01.017.

Raffel, M., Willert, C., Wereley, S., & Kompenhans, J. (2007). *Particle Image Velocimetry*. Springer.

Roshko, A. (1954). *On the drag and shedding frequency of two-dimensional bluff bodies.* Nasa.

Sahin, S., Durhasan, T., Pinar, E., & Akilli, H. (2021). Experimental study on passive flow control of circular cylinder via perforated splitter plate. *Wind and Structures*, *32*(6), 613-621. https://doi.org/10.12989/WAS.2021.32.6.613

Sheng, J., Meng, H., & Fox, R. (2000). A large eddy PIV method for turbulence dissipation rate estimation. *Chemical Engineering Science*, *55*(20), 4423-4434. https://doi.org/https://doi.org/10.1016/S0009-2509(00)00039-7

Shukla, S. G. R. (2023). Flow over a circular cylinder with a flexible splitter plate. *Journal of Fluid Mechanics*, *973*(A19). https://doi.org/doi:10.1017/jfm.2023.755

Shukla, S., Govardhan, R. N., & Arakeri, J. H. (2009). Flow over a cylinder with a hinged splitter plate. *Journal of Fluids and Structures*, 713-720. https://doi.org/doi:10.1016/j.jfluidstructs.2008.11.004

Tabatabaeian, S. M. (2015). Experimental Study of the flow field around a circular cylinder using plasma actuators. *Journal of Applied Fluid Mechanics*, *8*(2), 291-299. https://doi.org/https://doi.org/10.18869/acadpub.jafm.67.221.21459

Teksin, S., & S. Yayla (2016). Effects of Flexible Splitter Plate in the Wake of a Cylindrical Body. *Journal of Applied Fluid Mechanics*, 3053-3059. https://doi.org/10.29252/jafm.09.06.25564

Weier, T. G. (1998). Xperiments on cylinder wake stabilization in an electrolyte solution by means of electromagnetic forces localized on the cylinder surface. *Experimental Thermal and Fluid Science*, (16), 84-91. https://doi.org/http://dx.doi.org/10.1016/S0894-1777(97)10008-5

Westerweel, J. (1993). *Digital particle image velocimetry: Theory and application* [PhD Thessis, Delft University Press].

Wu, J., Shu, C., & Zhao, N. (2014). Numerical study of flow control via the interaction between a circular cylinder and a flexible plate. *Journal of Fluids and Structures*, (49), 594-613. https://doi.org/10.1016/j.jfluidstructs.2014.06.002

Zhu, H., Chen, Q., Tang, T., Alam, M. M., & Zhou, T. (2023). Flow structures around a circular cylinder with bilateral splitter plates and their dynamic characteristics. *Ocean Engineering, 269*. https://doi.org/https://doi.org/10.1016/j.oceaneng.2022.113547